Pergamon

Scripta Materialia, Vol. 40, No. 2, pp. 159–164, 1999
Elsevier Science Ltd

1359-6462/99 $20.00 + .00

PII S1359-6462(98)00404-7

HIGH-RATE DEFORMATION OF SINGLE CRYSTAL TANTALUM: TEMPERATURE DEPENDENCE AND LATENT HARDENING

Rajeev Kapoor, and Sia Nemat-Nasser
Center of Excellence for Advanced Materials, University of California, San Diego, La Jolla, CA 92093-0416, USA

(Received October 7, 1998)
(Accepted October 13, 1998)

Introduction

Latent hardening is defined as the hardening on a secondary slip system caused by slip on a primary slip system. Latent hardening is usually quantified by a latent hardening ratio (LHR) = τ_s/τ_p, where τ_p is the shear stress on the primary system just before unloading, and τ_s is the yield shear stress on the secondary system. Previous latent-hardening experimental work on bcc (1,2) and on fcc metals (3–6) has predominantly been carried out at quasi-static strain rates. In most of the previous studies, the LHR was observed to range from 1.1 to 2.5; the exceptions are the works by Nowacki and Zarka (7), Wu *et al*. (8), and Mingzhang *et al*. (9). In both bcc and fcc materials, coplanar systems experience essentially no latent hardening (1,3,6). In most studies the yield stress of latent systems was measured by back extrapolating the flow stress to zero plastic strain. According to Wu *et al*. (8) and Mingzhang *et al*. (9), the back extrapolation method is not an accurate measure of the yield stress of a latent system, because here the initial rapid work-hardening rate is ignored. Mingzhang *et al*. (9) measured τ_p as the stress at which deviation from linearity occurred, and almost always obtained a LHR less than 1. Stroh (10) calculated the stress field for a general distribution of dislocations on the primary and secondary slip system. From this he derived the LHR to be less than 1 for all combinations of the primary and latent slip systems. Similarly Zarka (11) calculated the far-field stresses created by randomly distributed segments of dislocations, and concluded that the LHR does not exceed 1.

The aim of the present research was to experimentally determine the LHR on the $\{211\}\langle 111\rangle$ slip systems of single-crystal tantalum during dynamic deformation. The temperature dependence of the $\{110\}$ and $\{211\}$ slip planes at these high strain rates was also determined.

Experiments

Two sets of experiments on single-crystal tantalum were carried out at an axial strain rate of 3000/s.

1. The temperature dependence of the shear stress of two slip systems, $(\bar{1}01)[111]$ and $(\bar{2}11)[111]$, was measured.
2. The latent hardening ratio on the $\{211\}\langle 111\rangle$ slip system was determined. The primary and secondary systems were chosen as $(\bar{2}11)[111]$ and $(211)[\bar{1}11]$, respectively.

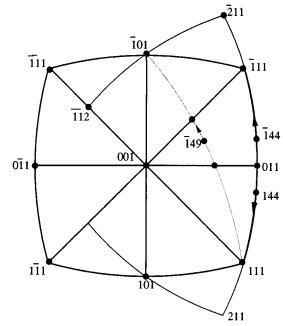

Figure 1. Stereographic projection with [001] as its pole. Shown here are the [$\bar{1}$49], the [$\bar{1}$44], and the [144] loading axes. Arrows show the direction the loading axis moves during compression.

A loading axis along the [$\bar{1}$49] direction produces a maximum shear stress on the ($\bar{1}$01)[111] slip system. A loading axis along the [$\bar{1}$44] direction produces a maximum shear stress on the ($\bar{2}$11)[111] slip system. Figure 1 shows part of a stereographic projection with [001] as its pole. Shown here are the [$\bar{1}$49], the [$\bar{1}$44], and the [144] loading axes with arrows indicating the direction in which the loading axes rotate during compression. The temperature dependence of the shear stress was measured by carrying out compression tests at an axial strain rate of 3000/s, on cuboidal specimens with approximate dimensions of 4.8mm $\times$ 3.6mm $\times$ 3.6mm.

Latent-hardening experiments were carried out with ($\bar{2}$11)[111] as the primary slip system, and the (211)[$\bar{1}$11] as the latent slip system. The directions [$\bar{2}$11], [111], [$\bar{1}$11], and [211] are coplanar, and lie on the (0$\bar{1}$1) plane, as seen in Figure 1. The samples were machined such that 2 of the 6 faces were parallel to the (0$\bar{1}$1) plane. Given that slip does occur on the ($\bar{2}$11)[111] slip system, and since both the ($\bar{2}$11) plane and the [111] direction are perpendicular to the (01$\bar{1}$) face, *the dimensions of the samples along the [01$\bar{1}$] direction do not change significantly during deformation*. Figure 2 is a schematic diagram showing the single-crystal sample (a) before deformation and (b) after deformation on the primary slip system up to a shear strain of about 0.18. The plane of the paper is the (01$\bar{1}$) plane. In Figure 2(c) and (d) are shown schematic diagrams of how samples with a loading direction along [144] and [$\bar{1}$44], respectively, were cut. The samples with loading direction along [$\bar{1}$44] were needed to check the effects of wire EDM (wire Electric Discharge Machining was the technique used to machine these samples).

The following latent-hardening experiments were carried out,

1. Single-crystal tantalum samples were deformed up to a shear strain of about 0.18, at 296K and 3000/s, along [$\bar{1}$44], so as to activate the primary slip system, ($\bar{2}$11)[111].
2. One of the samples was cut so as to keep the loading axis along [$\bar{1}$44].* This reactivates the primary slip system, and was done as a measure of checking. See Figure 2(d).
3. The remaining samples were cut so as to obtain a loading axis along [144]. See Figure 2(c).
4. One sample from each of the loading directions was deformed at 296K and 3000/s.
5. Temperature dependence of the reload stress for samples deformed on the latent slip system, (211)[$\bar{1}$11], was also measured.

*It should be noted that the rotation of the crystal after a shear strain of about 0.18 is 6° wand was taken into account while cutting the crystal.

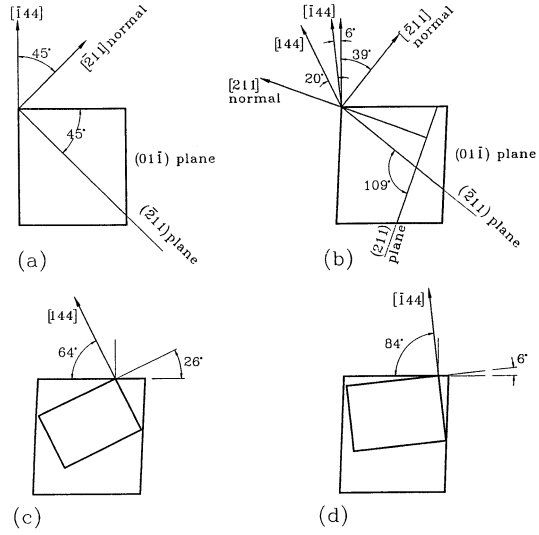

Figure 2. Schematic diagram of samples with the $(01\bar{1})$ face; (a) undeformed sample with loading direction along $[\bar{1}44]$, showing the $(\bar{2}11)$ plane; (b) sample deformed up to 0.18 shear strain, showing the rotated $[\bar{1}44]$ direction, the [144] direction, the $(\bar{2}11)$ and the (211) planes and their corresponding normals; (c) sample cut for reloading along the [144] direction; (d) sample cut or reloading along the $[\bar{1}44]$ direction.

High strain rates of 3000/s were achieved using a split Hopkinson pressure bar with a momentum trap (12). In order to carry out high-temperature tests using the Hopkinson bar, the apparatus was modified, such that minimal heating of the incident and transmission bars takes place (13).

Results and Discussion

Temperature Dependence

From the compression tests carried out on single-crystal tantalum, the axial strain and axial stress (σ) were converted to shear strain (γ) and shear stress (τ), using the following equations (14),

$$\gamma = \frac{1}{\cos\theta_o}\left[\sin\theta_o - \sqrt{\left(\frac{h}{h_o}\right)^2 - \cos^2\theta_o}\right] \text{ and } \tau = \sigma\frac{h}{h_o}\cos\theta_o\sqrt{1-\left(\frac{h}{h_o}\cos\theta_o\right)^2},$$

where h_o is the initial height of the sample, h is the deformed height of the sample, and θ_o is the initial angle the loading axis makes with the slip plane normal, which in the present case is 45°. Note that the above equations apply only as long as one slip system is active. A plot of the resolved shear stress at 0.1 shear strain vs. temperature is shown in Figure 3. There are 2 curves shown in this graph, one for samples loaded along $[\bar{1}44]$ such as to activate the $(\bar{2}11)[111]$ slip system, and the other for samples loaded along $[\bar{1}49]$ such as to activate the $(\bar{1}01)[111]$ slip system. The temperature dependence of the resolved shear stress for these two slip systems is similar, indicating that these two slip systems have similar short range barriers.

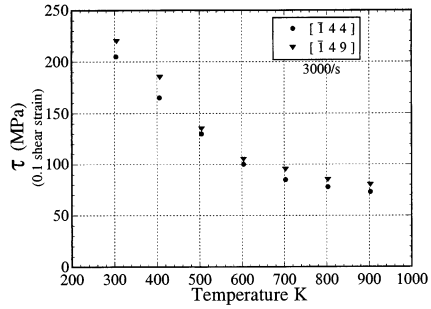

Figure 3. Shear stress at 0.1 shear strain vs. temperature for single-crystal tantalum samples deformed at 3000/s along [$\bar{1}$44] and [$\bar{1}$49].

Latent Hardening

Figure 4 is a shear stress vs. shear strain plot showing the reload stress on the latent slip system, (211)[$\bar{1}$11]. Shown here are curves for, (1) a sample deformed along the [$\bar{1}$44] direction up to a large strain, (2) a sample deformed along the [$\bar{1}$44] direction up to a small shear strain of 0.18, unloaded, and reloaded along the [144] direction, and (3) a sample deformed along the [$\bar{1}$44] direction up to a small strain of 0.18, unloaded, and reloaded along the [$\bar{1}$44] direction. It is observed that if cuboidal samples are deformed beyond shear strains of 0.25, deformation starts to localize along one of the diagonals. This leads to an apparent drop in the macroscopic flow stress. In Figure 4 such a drop in load is observed for the sample deformed up to a large strain. In the present latent-hardening experiment, the sample was unloaded before any such localization became important. The reload shear stress on the latent system, (211)[$\bar{1}$11], was higher than the reload shear stress on the primary system, ($\bar{2}$11)[111], by 10%, that is, the LHR was 1.10. These experiments were repeated and the LHRs obtained were 1.12 and 1.07.

Latent hardening can arise due to an increase in either the athermal stress component, τ_a, or the thermal stress component, τ^*. It is assumed that at high strain rates, the shear stress, τ, is the sum of τ^* and τ_a (13,15,16). In order to check the cause of hardening, the preloaded samples (samples loaded along [$\bar{1}$44] were reloaded along [144]) at various temperatures. The reload shear stress is plotted as a function of temperature in Figure 5. For comparison, the shear stress of samples deformed along [$\bar{1}$44] after a shear strain of 0.18 is also plotted.

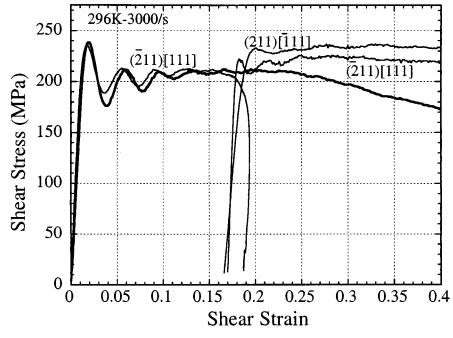

Figure 4. Shear stress-shear strain plot of single crystal tantalum tested to study latent hardening. ($\bar{2}$11)[111] is the primary slip system, and (211)[$\bar{1}$11] is the latent slip system.

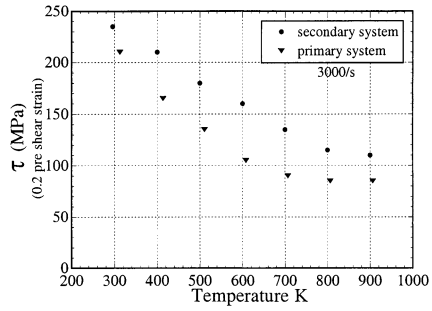

Figure 5. Shear stress plotted as function of temperature for the primary, $(\bar{2}11)[111]$, as well as the latent, $(211)[\bar{1}11]$, slip system.

As seen from Figure 5, for all of the tested temperatures, the shear stress of the latent system after a prestrain of about 0.18 is higher than the shear stress of the primary system after a strain of 0.18. For both the primary and the latent slip systems, τ^* becomes 0 beyond 900K, resulting in τ_a = 110 MPa for the latent system, and τ_a = 85 MPa for the primary system. Thus, from the present set of experiments, it is certain that τ_a for the latent slip system is higher than that for the primary system. Whether the thermal stress on the secondary system also changes is a matter of further investigation. Kocks and Brown (3) explained that latent hardening in fcc metals arose because dislocations have to overcome impenetrable point obstacles, such as intersections of forest dislocations by active mobile dislocations. The traces of the $(\bar{2}11)$ and the (211) planes on the $(01\bar{1})$ plane are shown schematically in Figure 6. $(\bar{2}11)$ and (211) are perpendicular to $(01\bar{1})$. From this diagram it is clear that these planes are intersecting slip planes, and any dislocation production on the primary plane will create a forest of dislocations on the secondary plane. If it is assumed that τ_a is caused by the far-field average value of the stresses due to dislocations, then according to the calculations performed by Stroh (10) and Zarka (11), τ_a should be less for the latent system than for the primary system. This is in contrast to the present experimental results, which suggest that the movement of dislocations and increase of dislocation density on the primary system causes an increase in the far-field stress for dislocations moving on the secondary systems. At this point, no conclusive reason can be provided as to why the athermal stress component should increase more on the latent system as compared to the primary system.

Conclusions

Temperature dependence of the shear stress of the $(\bar{2}11)[111]$ and that of the $(\bar{1}01)[111]$ slip systems were found to be very similar. Latent-hardening tests were carried out on single-crystal tantalum with $(\bar{2}11)[111]$ as the primary slip system and $(211)[\bar{1}11]$ as the latent slip system. After a pre-shear strain

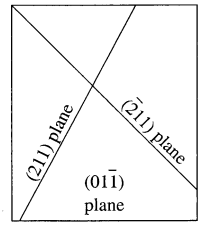

Figure 6. Schematic representation of relative positions of the two planes.

of about 0.18, the LHR was observed to be about 1.10. The athermal shear stress component for the latent system was observed to be larger than that for the primary system, suggesting that latent hardening primarily arises because of an increase in the athermal stress component.

Acknowledgements

This work was supported by the Army Research Office (ARO) Contract, DAAL 03-92-G-0108 to the University of California, San Diego.

References

1. Y. Nakada and A. S. Keh, Acta Metall. 14, 961 (1966).
2. P. Franciosi, Acta Metall. 31, 1331 (1983).
3. U. F. Kocks and T. J. Brown, Acta Metall. 14, 87 (1966).
4. E. J. H. Wessels and P. J. Jackson, Acta Metall. 17, 241 (1969).
5. S. I. Hong, H. Inui, and C. Laird, Acta Metall. Mater. 40, 397 (1992).
6. H.-M. Wu, M. A. Przystupa, and A. L. Ardell, Metall, Mater. Trans. A. 28A, 2353 (1997).
7. W. K. Nowacki and J. Zarka, Int. J. Solids Struct. 7, 1277 (1971).
8. T. Y. Wu, J. L. Bassani, and C. Laird, Proc. Roy. Soci. London A. 435, 1 (1991).
9. W. Mingzhang, L. Shi, L. Chenhua, W. Zhongguang, and X. Jimei, Scripta Mater. 35, 1183 (1996).
10. A. N. Stroh, Proc. Phys. Soc. B66, 2 (1953).
11. J. Zarka, in Constitutive Equations in Plasticity, ed. A. S. Argon, pp. 359–385, the MIT Press, Cambridge, MA 1st edn. (1975).
12. S. Nemat-Nasser, J. B. Isaacs, and J. E. Starrett, Proc. Roy. Soci. London A. 435, 371 (1991).
13. S. Nemat-Nasser and J. B. Isaacs, Acta Mater. 45, 907 (1997).
14. C. N. Reid, Deformation Geometry for Materials Scientists, Pergamon Press, New York (1973).
15. S. Nemat-Nasser, T. Okinaka, and L. Ni, J. Mech. Phys. Solids, 46, 1009 (1998).
16. P. S. Follansbee and U. F. Kocks, Acta Metall. 36, 81 (1988).